FULL PAPER

Magnetic Resonance in Medicine 00:00–00 (2014)

Noise Propagation in Region of Interest Measurements

Michael S. Hansen,[1]* Souheil J. Inati,[2] and Peter Kellman[1]

Purpose: The purpose of this work was to develop and validate a technique for predicting the standard deviation (SD) associated with thermal noise propagation in region of interest measurements.

Theory and Methods: Standard methods for error propagation estimation were used to derive equations for the SDs of linear combinations of complex, magnitude, or phase pixel values. The equations were applied to common imaging scenarios in which the image pixels were correlated due to anisotropic pixel resolutions and parallel imaging. All SD estimates were evaluated efficiently using only vector–vector multiplications and Fourier transforms. The estimated SDs were compared to those obtained using repeated experiments and pseudo replica reconstructions.

Results: The proposed method was able to predict region of interest SDs in all the tested analysis scenarios. Positive and negative noise correlations caused by different parallel-imaging aliasing point spread functions were accurately predicted, and the method predicted the confidence intervals (CI) of time-intensity curves for in vivo cardiac perfusion measurements.

Conclusion: An intuitive technique for region of interest CIs was developed and validated using phantom experiments and in vivo data. **Magn Reson Med 000:000–000, 2014. © 2014 Wiley Periodicals, Inc.**

Key words: region of interest measurement; standard deviation; confidence interval; signal to noise ratio; parallel imaging

INTRODUCTION

Diagnostic interpretation of MR images frequently involves region of interest (ROI) measurements. An important component of ROI analysis is to determine the average (or sum) pixel intensity in a specific area of the image, for example, to compare signal intensities in a suspected lesion with signal intensities in normal tissue. More generally, the objective is to determine the value of some linear combination of the pixel values in an image region. For such an analysis, it is desirable to know the variability of the estimate caused by thermal noise. The standard deviation (SD) (σ) or variance (σ^2) of each individual pixel can be estimated directly from the raw data and noise samples for most Cartesian linear reconstructions using the techniques developed for signal-to-noise (SNR) scaled reconstruction (1,2). An alternative method to obtain pixel-wise noise variance estimates is the pseudo replica technique proposed by Robson et al. (3) or the faster approximation based on only a few pseudo replicas introduced by Weins et al. (4). If the pixels are assumed to be uncorrelated, the variance of the sum of the pixels in an ROI is simply the sum of the variances of each of the individual pixels in the ROI. In most practical imaging experiments, the pixels are correlated, which makes it more challenging to determine the SD of the average pixel intensity in an ROI. In some simple cases, it may be possible to determine the effective number of independent pixels in the region of interest and calculate a factor to scale an estimate of the ROI SD accordingly. However, in the general case, the pixel correlation in an ROI is affected by several interacting factors, such as reduced phase-encoding resolution, partial Fourier acquisition, raw data filtering, and parallel imaging (5–7). Moreover, the orientation of the ROI also plays a role; that is, a given ROI may have a different SD if oriented along the phase-encoding direction—as opposed to along the frequency-encoding direction. This latter point makes it difficult to use a global pixel correlation factor to scale SD estimates.

The SD of an ROI measurement in general can be determined using the pseudo replica technique (3). With this technique, multiple reconstructions (replicas) are obtained by adding noise to the original raw data and repeating the reconstruction. The SD in each pixel is obtained as the SD across the replicas; and similarly, one can determine the SD for an ROI measurement (sum or average) by repeating the ROI measurement on each replica and calculating the SD of the results. Although this technique has many advantages in terms of generally applicability and simplicity, it is time-consuming and difficult to integrate with an image analysis workflow. The faster method for pixel-wise noise estimation (4) employs the averaging of a neighborhood of pixels to improve precision of noise variance estimates. This approach does not capture the noise correlation between pixels within an ROI. In this article, the original pseudo replica method has been used as reference standard.

The purpose of this article is to demonstrate a practical technique for calculating the SD of any linear combination of the pixels in an MR image without the need for repeated reconstructions. The techniques can be applied to most Cartesian linear reconstructions, and it can be used to determine SDs for ROI measurements of real, imaginary, magnitude, and phase components of the complex images.

THEORY

The goal of the ROI measurement is to obtain some linear combination of the pixels in the image. If $\boldsymbol{\rho}$ is a column

[1]National Heart, Lung, and Blood Institute, National Institutes of Health, Bethesda, Maryland, USA.

[2]National Institute of Mental Health, National Institutes of Health, Bethesda, Maryland, USA.

*Correspondence to: Michael S. Hansen, National Heart, Lung, and Blood Institute National Institutes of Health, Building 10, B1D405, 9000 Rockville Pike, Bethesda, MD 20814. E-mail: michael.hansen@nih.gov

Received 7 January 2014; revised 29 January 2014; accepted 6 February 2014

DOI 10.1002/mrm.25194

Published online 00 Month 2014 in Wiley Online Library (wileyonlinelibrary.com).

vector containing all the pixels of the image and $\mathbf{m}$ is a column vector containing linear weighting coefficients corresponding to each pixel, then the result r (scalar) of an ROI measurement can be written as:

$$r = \mathbf{m}^{\mathbf{H}}\boldsymbol{\rho} \quad [1]$$

In general the variance of r is:

$$\sigma_r^2 = \mathbf{m}^{\mathbf{H}}\boldsymbol{\Sigma}_{\boldsymbol{\rho}}\mathbf{m} \quad [2]$$

Where $\boldsymbol{\Sigma}_{\boldsymbol{\rho}}$ is the covariance matrix of the pixel noise. In the rare case in which the pixels are uncorrelated, $\boldsymbol{\Sigma}_{\boldsymbol{\rho}}$ is a diagonal matrix with the noise variance of each pixel along the diagonal. In most ROI measurements, $\mathbf{m}$ would be a vector with entries of either "1" (for pixels within the ROI) or "0" (for pixels outside the ROI). However, it need not be a binary mask. If a certain region of the image should be weighted differently in the analysis, the coefficients can be adjusted accordingly. The covariance matrix $\boldsymbol{\Sigma}_{\boldsymbol{\rho}}$ is a large matrix that would be impractical to form directly for most real experiments, but it is possible to obtain an expression for it using the knowledge that, if covariance matrix of some vector $\mathbf{x}$ is $\boldsymbol{\Sigma}_{\mathbf{x}}$, then the covariance matrix of the linear transform $\mathbf{Ax}$ is $\mathbf{A}\boldsymbol{\Sigma}_{\mathbf{x}}\mathbf{A}^{\mathbf{H}}$. This is the general form used to obtain Eq. [2]. If the covariance matrix of the noise in the acquired k-space samples is denoted $\boldsymbol{\Sigma}_{\mathbf{k}}$, and the linear image reconstruction (image formation) process is defined by the matrix $\mathbf{F}$, then Eq. [2] can be written as:

$$\sigma_r^2 = \mathbf{m}^{\mathbf{H}}\mathbf{F}\boldsymbol{\Sigma}_{\mathbf{k}}\mathbf{F}^{\mathbf{H}}\mathbf{m} \quad [3]$$

In general, it is straightforward to ensure that $\boldsymbol{\Sigma}_{\mathbf{k}}$ is diagonal or even identity. Specifically, if noise prewhitening is performed as described in (1,8), and any oversampling in the readout direction is removed by Fourier-transform to image space, field of view (FOV) reduction, and Fourier transform back to k-space, the k-space noise covariance matrix, $\boldsymbol{\Sigma}_{\mathbf{k}}$ will be diagonal or identity in the case of uniform k-space sampling. For Cartesian acquisitions using phased array coils, the image formation matrix $\mathbf{F}$ can be split into a set of operations that are either vector–vector multiplications or Fourier transform operations. Specifically, $\mathbf{F}$ would consist of a) a k-space masking operation, which would account for any undersampled areas (reduced resolution or parallel imaging) and raw data filtering; b) Fourier transform to image space; and c) pixel-wise, linear combination of data from multiple receive channels. The latter operation would take the form:

$$\rho(x) = \sum_{i=1}^{\Gamma} u_i(x)a_i(x) \quad [4]$$

Where $\rho(x)$ is the reconstructed image pixel at location x, $u_i(x)$ is the phased array combining (or unmixing) coefficient for coil i at location x; $a_i(x)$ is the pixel value (after Fourier transform) in coil i at location x; and Γ is the number of coils. The coil pixel values $a_i(x)$ could contain aliasing in the case of parallel imaging, and $u_i(x)$ will be the set of coefficients that produce unaliased and SNR optimal images (in some sense defined by the parallel imaging approach). Both sensitivity-encoding (SENSE) (6) and generalized autocalibrating partially parallel acquisitions (GRAPPA) (7) type parallel reconstruction algorithms can be expressed as unmixing with a phased array combiner. The multiplication with $\mathbf{F}^{\mathbf{H}}$ would be: a) multiplication of the image with the conjugate of the unmixing coefficients u_i (this generates multiple image channels from a single image); b) Fourier transform to k-space; and c) k-space masking. Based on the operations described above, it is possible to obtain the variance of a linear combination of pixels in a complex image.

It is common to perform the ROI measurements on a magnitude or phase image. The magnitude or phase operators are not linear operations; consequently, Eq. [3] cannot be applied directly. The method presented in this article employs a linear approximation of this nonlinear operation, which is valid in the case of moderate and high SNR ratios. The approximation follows commonly used principles uncertainty propagation, for example (9,10). Let $\mathrm{T}(\mathbf{x})$ be a function (linear or nonlinear) such that $\mathbf{y} = \mathrm{T}(\mathbf{x})$, then $\mathbf{y}$ can be approximated by:

$$\mathbf{y} \approx \mathrm{T}(\mathbf{x}_0) + \mathbf{J}(\mathbf{x} - \mathbf{x}_0) \quad [5]$$

Where $\mathbf{J}$ is the Jacobian of T at $\mathbf{x_0}$. Using this, the covariance matrix of $\mathbf{y}$, $\boldsymbol{\Sigma}_{\mathbf{y}}$, can be approximated:

$$\boldsymbol{\Sigma}_{\mathbf{y}} \approx \mathrm{E}\left\{(\mathbf{y} - \mathbf{y}_0)(\mathbf{y} - \mathbf{y}_0)^{\mathrm{H}}\right\} \quad [6]$$

$$\approx \mathrm{E}\left\{(\mathbf{J}(\mathbf{x} - \mathbf{x}_0))(\mathbf{J}(\mathbf{x} - \mathbf{x}_0))^{\mathrm{H}}\right\} \quad [7]$$

$$\approx \mathbf{J}\boldsymbol{\Sigma}_{\mathbf{x}}\mathbf{J}^{\mathrm{H}} \quad [8]$$

Where $\mathrm{E}\{\cdot\}$ denotes the expected value. Equation [8] allows an approximation of the variance, even in the case of nonlinear transformations as long as an estimate of the Jacobian is known. If the operation of taking the magnitude is approximated as a pixel-wise phase change to rotate the complex pixel signal to be oriented along the real axis, the variance of a linear combination of the magnitude image pixels can be approximated as:

$$\sigma^2_{magroi} = \mathbf{m}^{\mathrm{H}}\boldsymbol{\theta}^{\mathrm{H}}\mathbf{F}\boldsymbol{\Sigma}_{\mathbf{k}}\mathbf{F}^{\mathrm{H}}\boldsymbol{\theta}\mathbf{m} \quad [9]$$

Where $\boldsymbol{\theta}$ is a diagonal matrix with complex numbers along the diagonal, with magnitude 1 and phase equal to some estimate of the image phase when the image has a well-defined phase (there is some signal), and zero otherwise. This is equivalent to a transformation of the covariance matrix to an in-phase/quadrature covariance matrix (11). Because the SD of the phase is approximately inversely proportional to the SNR (at moderate to high SNR), an expression of the uncertainty of the phase can be found to be:

$$\sigma^2_{phaseroi} = \mathbf{m}^{\mathrm{H}}\boldsymbol{\theta}^{\mathrm{H}}\mathbf{M}\mathbf{F}\boldsymbol{\Sigma}_{\mathbf{k}}\mathbf{F}^{\mathrm{H}}\mathbf{M}\boldsymbol{\theta}\mathbf{m} \quad [10]$$

Where $\mathbf{M}$ is a diagonal matrix with $1/|\rho|$ (the reciprocal of the signal magnitude) along the diagonal. Clearly this will not be well-defined in regions of very low signal.

The results in Eqs. [9] and [10] can be obtained through other simpler analyses than the formalism outlined in Eqs. [6] to [8], which applies in general for any

nonlinear approach to pixel estimation. Because the Jacobian can be used for cases in which the pixel intensities have obtained through more complicated nonlinear estimation procedures (e.g., parametric mapping), it is included here for completeness.

Equations [3], [9], and [10] provide a way to obtain the variance or SD of an ROI measurement. Equation [3] can be used to estimate the variance when analyzing complex images, and Eqs. [9] and [10] would be used to analyze magnitude or phase images respectively. The variances can be calculated directly without the need to form pseudo replicas. Moreover, the evaluation of those equations can be done using vector–vector multiplications and Fourier transforms alone, and the large covariance matrices need not to be formed or stored explicitly. In the following sections, practical methods for working with the proposed solution will be outlined, and the methods will be demonstrated on phantom and in vivo data.

METHODS

Image Reconstruction and Analysis

The methodology outlined in this article does not rely on a particular reconstruction procedure as long as the operations contained in the image formation matrix **F** are known. However, the reconstruction used in the experiments is outlined here for clarity. Figure 1 illustrates an overview of the reconstruction pipeline. For all experiments, noise samples were acquired and used to calculate a noise prewhitening matrix, which was applied to all acquired data (1). Any readout oversampling was then removed from the data by Fourier transform to image space, FOV reduction, and Fourier transform back to k-space. After these first two steps, the k-space data was considered to have unit noise variance, and the noise was considered uncorrelated between channels and also between sample locations in k-space. The data was then Fourier transformed from k-space to image space to form individual channel images. These individual channel images were combined with a set of channel combination or unmixing coefficients, as described in Eq. [4]. These coefficients were calculated from calibration data, which were either acquired inline with the data or obtained as a time average of the data (12). A GRAPPA calibration was used to calculate k-space convolution kernels. These kernels were zero-padded to the full matrix size and Fourier transformed to image space, where the image space kernels for each individual channel were combined using coil-sensitivity maps estimated from the calibration data using the method outlined by Walsh et al. (13). To enable validation of the method outlined in this article, multiple pseudo replicas were also generated by adding noise with unit variance to the data and repeating the reconstruction. In all image reconstruction steps, scaling was applied to ensure that unit noise variance was maintained (1). Specifically, scale factors were applied to account for the number of independent samples in the Fourier transforms, and scale factors were applied to account for raw data filters, etc. As a result, the reconstructed images had noise variance equal to 1 in each pixel, except in the cases in which parallel imaging was employed (see below); here the noise variance in in each pixel was scaled according to the g-factor (6).

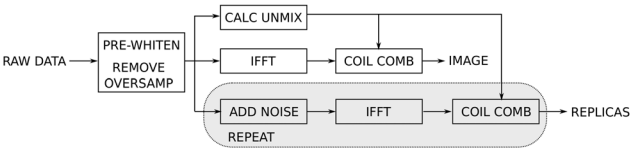

FIG. 1. Reconstruction pipeline. Data is first prewhitened to ensure unit noise variance, and that noise is uncorrelated between receive channels. Any readout oversampling is also removed from the data. Calibration data is processed to calculate unmixing coefficients, and the remaining data is Fourier transformed to image space where the channel images are combined using the unmixing coefficients. In a parallel pipeline, noise with unit variances is repeatedly added to the raw data, and pseudo replicas are reconstructed.

With such a noise-scaled reconstruction, the SD of the sum or the mean of an ROI has a predictable behavior in reconstructions in which the noise is uniformly distributed in the image (no parallel imaging) and there is no correlation between the image pixels. This is illustrated in Figure 2 for a reconstruction in which all the pixels are independent and no parallel imaging is used. The left panel shows a plot of the SD of the sum of the pixel magnitudes in an ROI as a function of the square root of the number of pixels. It is a linear function with slope 1 for both the SD predicted by Eq. [9] and the result of a pseudo replica experiment. The right panel is a more familiar illustration of the same point; a plot of the SD of the mean of an ROI against the number of pixels is a straight line on a log–log plot (i.e., the SD decreases proportionally to the square root of the number of pixels). In reconstructions in which the pixels are correlated, these plots could deviate from a straight line and/or the slope would be different. The following experiments are intended to illustrate these deviations due to pixel correlations and the proposed methods ability to predict them.

Phantom Experiments

A spherical, oil-filled phantom was scanned with an RF spoiled gradient echo sequence with the following parameters: matrix 128 × 128, FOV 300 × 300 mm, repetition time (TR) 3.0 ms, and echo time (TE) 1.5 ms. Twenty receive coils were used. The acquired k-space was fully sampled, and 100 repetitions (with a 10 s pause between each repetition) were acquired. The phantom data was used to probe the proposed techniques' ability to predict ROI SDs for two commonly used imaging techniques.

First, a reduced phase-encoding direction resolution of 50% (effective sampled matrix 128 × 64) was simulated. An ROI with a fixed width of 10 pixels and increasing length from 1 to 80 (to fit inside the spherical phantom) was defined and placed with the length direction either along the frequency-encoding direction or along the phase-encoding direction. Figure 3 is an illustration of the spherical phantom image (fully sampled) with the maximum length ROI placed along the phase-encoding direction. The gray scale on the image is in units of

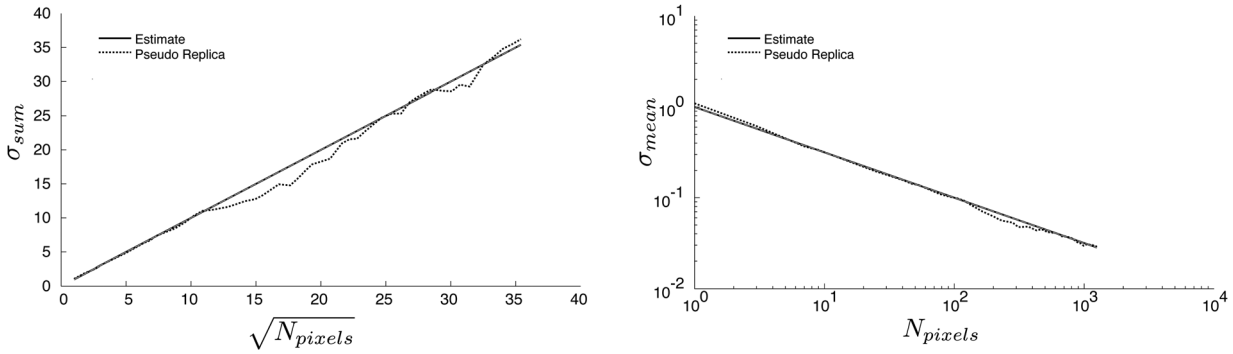

FIG. 2. An illustration of the relationship between the standard deviation of a magnitude region of interest and the number of pixels for a reconstruction in which all pixels are independent and no parallel imaging was employed. The left plot shows the sum of the pixel magnitudes as a function of the square root of the number of pixels in a linear coordinate system. The right plot shows the mean of the pixel magnitudes as a function of the number of pixels in a log–log coordinate system.

SNR, the average SNR in the depicted ROI is ~15 for the fully sampled image. For each length of the ROI, the SD of the sum and the mean of the ROI was calculated based on a) the proposed technique, b) pseudo replica technique (100 replicas), and c) the 100 actual repetitions of the experiment. The results were plotted for the analysis of the magnitude or the phase of the image.

The purpose of the second experiment was to investigate the effects of parallel imaging. The acquired phantom data was undersampled by a factor of 4 in the phase-encoding direction. Two different undersampling patterns were investigated: In one undersampling pattern, lines 1, 5, 9, 13, ... were "acquired"; in another undersampling pattern, lines 3, 7, 11, 15, ... were acquired. The purpose of this experiment was to illustrate the effects of different point spread functions due to sampling phase on the noise correlation in an ROI. For the parallel imaging experiments, the phase-encoding direction resolution was 100%, and the ROI sizes and orientations were the same as in the phase-encoding resolution experiment.

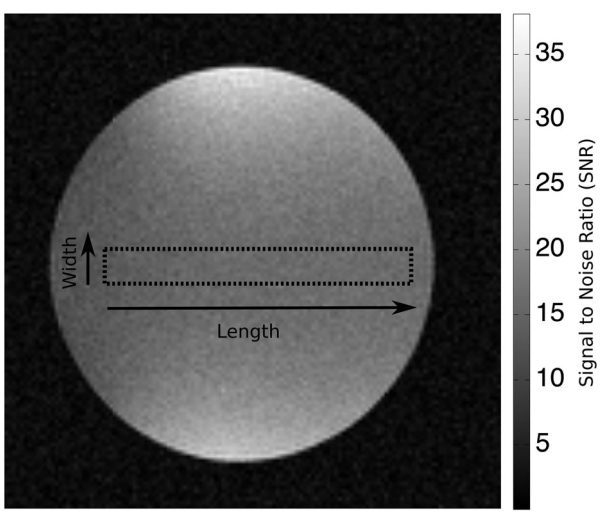

FIG. 3. Illustration of the spherical phantom used in the phantom experiments. The reconstruction depicted is for fully sampled data, and the dotted line outlines the largest region of interest (ROI) analyzed. The ROI is oriented along the phase-encoding direction. The gray scale is in units of signal to noise (SNR), and the average SNR in the depicted ROI is ~15.

In Vivo Experiments

To demonstrate the proposed techniques ability to predict SDs of ROI measurements on in vivo images, an example from myocardial stress perfusion measurements was chosen. A patient with a transmural septal perfusion defect was imaged during the infusion of a bolus of Gd-based contrast agent. The local institutional review board approved the study protocol and the patient gave written informed consent. A combination of a spine array coil and a surface array coil was used for signal reception. A total of 30 coil elements were used. A short axis slice through the heart was imaged with a saturation recovery (SR)-prepared, single shot steady-state free precession perfusion sequence. The acquired matrix size was 192 × 110 and the FOV was 360 × 270 mm. Partial Fourier (asymmetric echo, 75%) was used in the readout direction, and a parallel imaging acceleration (rate 2) was used with a time-interleaved sampling pattern (14) to enable calibration from a time average of the data. The phase-encoding direction was anterior–posterior. TE was 1.03 ms and TR time was 3.03 ms. Total acquisition time per frame was 167 ms, including saturation recovery time; and a total of 60 time frames were acquired, one every heartbeat for 60 heartbeats. The initial 2 frames had proton density weighting acquired at a lower excitation flip angle without SR prep in order to correct for spatial variation in surface coil intensity. The proton density images were used to calculate the average proton density signal in the ROIs used in the image analysis. The proton density ratio between the analyzed ROIs was used to scale the ROI weights, that is, it was used to modify $\mathbf{m}$ in Eq. [9] to correct for surface coil sensitivity variations between ROIs.

The images for each frame were reconstructed as outlined in Figure 1. In the in vivo case, it was not practical to repeat the actual experiment 100 times, but 100 pseudo replicas were reconstructed. Two ROIs were drawn on the short axis image. One ROI covered the

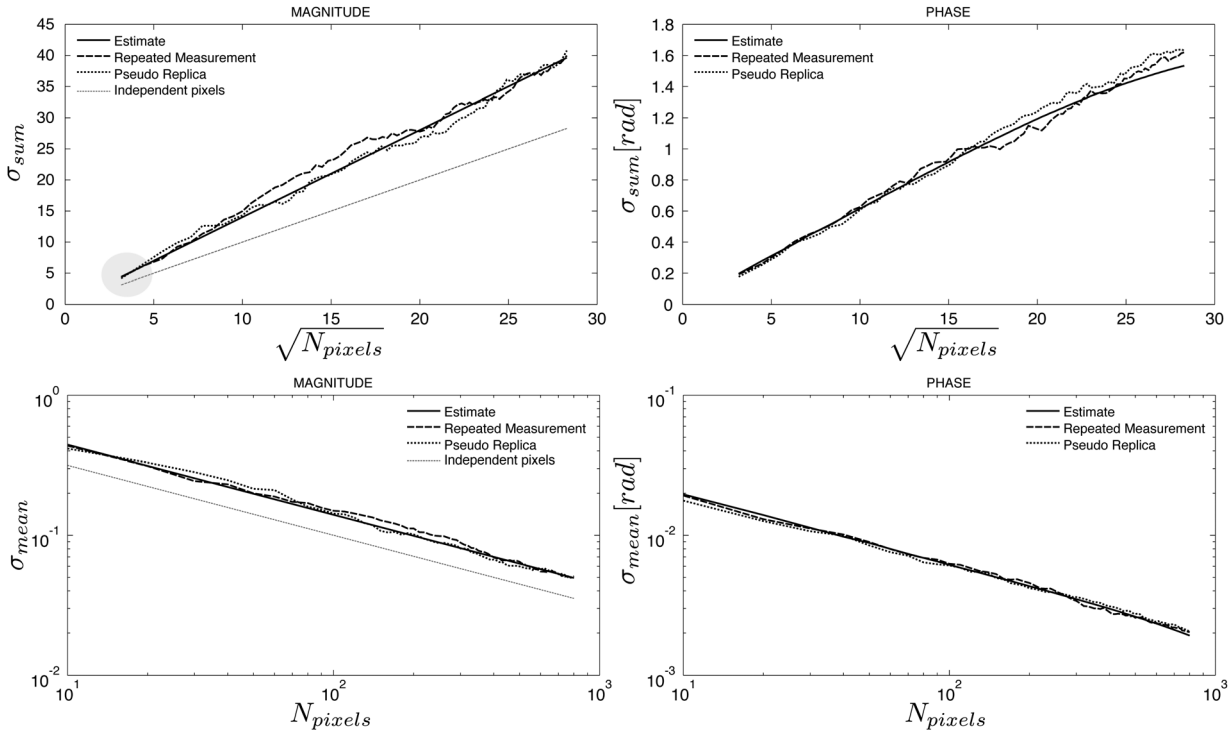

FIG. 4. Measured and predicted standard deviations (SD) of the sum (top row) and mean (bottom row) of a region of interest (ROI) as a function of the number of pixels in the ROI as it grows along the *readout* direction in an image with reduced effective resolution in the phase-encoding direction. The solid line is the predicted SD from the proposed method. The dashed line is the calculated SD from 100 repeated experiments. The dotted line is the calculated SD from 100 pseudo replica reconstructions. The gray dotted line on the magnitude plots indicates that the predicted SD when assuming that all pixels are independent. The gray circle highlights the initial region of the curve, whereas the actual SDs deviate from the gray line because even an ROI with length 1 has dependencies between the pixels. This should be compared to Figure 5, in which the pixels of an ROI with length 1 are actually independent.

septum with the perfusion defect and the other covered the healthy left ventricular muscle. Each ROI took up about one-half of the left ventricle. The position of the ROIs was adjusted manually for respiratory motion on each of the 60 frames. The SD of the signal intensities on both normal and ischemic regions was predicted with the proposed method and calculated based on the 100 pseudo replica reconstructions.

RESULTS

Figures 4 and 5 show the results of the phantom experiment with reduced phase-encoding resolution. In Figure 4, an ROI with a width of 10 pixels was increased in length along the frequency-encoding direction from 1 pixel up to 80 pixels. It can be seen that for the ROI with length of 1 pixel, there is already a discrepancy between the SD predicted by the pixel-wise SD and the combined SD for the ROI. This is caused by the correlation between pixels in the phase-encoding direction, resulting from the inherent use of interpolation to create square pixels, although the true resolution is reduced in the phase-encoding direction. As the length of the ROI increases, the SD of the sum increases linearly with the square root of the number of pixels. In Figure 5, the ROI is placed orthogonal to the ROI used in Figure 4. Consequently, the prediction of the SD based on the pixel-wise SD is in agreement with the predicted and measured SDs when the ROI is only 1 pixel long (because all pixels are independent in the frequency encode direction). As the ROI grows, the SD of the sum goes up linearly with the square root of the number of pixels, but it grows faster than it would if the pixels were independent. In all cases, the predicted SD and the measured by repeated experiments or pseudo replicas are in good agreement.

Figures 6 and 7 show the results of applying parallel imaging (rate 4) to the phantom experiment. Two different sampling patterns were used to illustrate the effects of the resulting different aliasing point spread functions. In both cases, the ROI increased in size along the phase-encoding direction; and when the ROI reached a size that is larger than FOV/4, the correlation in the noise caused by the aliasing point spread function takes effect. In both cases, the SD of the ROI starts to deviate from what would be predicted by the g-factor alone; however, in one case (Fig. 7) the noise actually decreases because pixels with negatively correlated noise are included in the ROI, and in the other case (Fig. 8) the SD is elevated from what would be expected due to positively correlated noise in pixels in the ROI. In all cases, the SDs predicted by the proposed method, and the actual measurements are in good agreement.

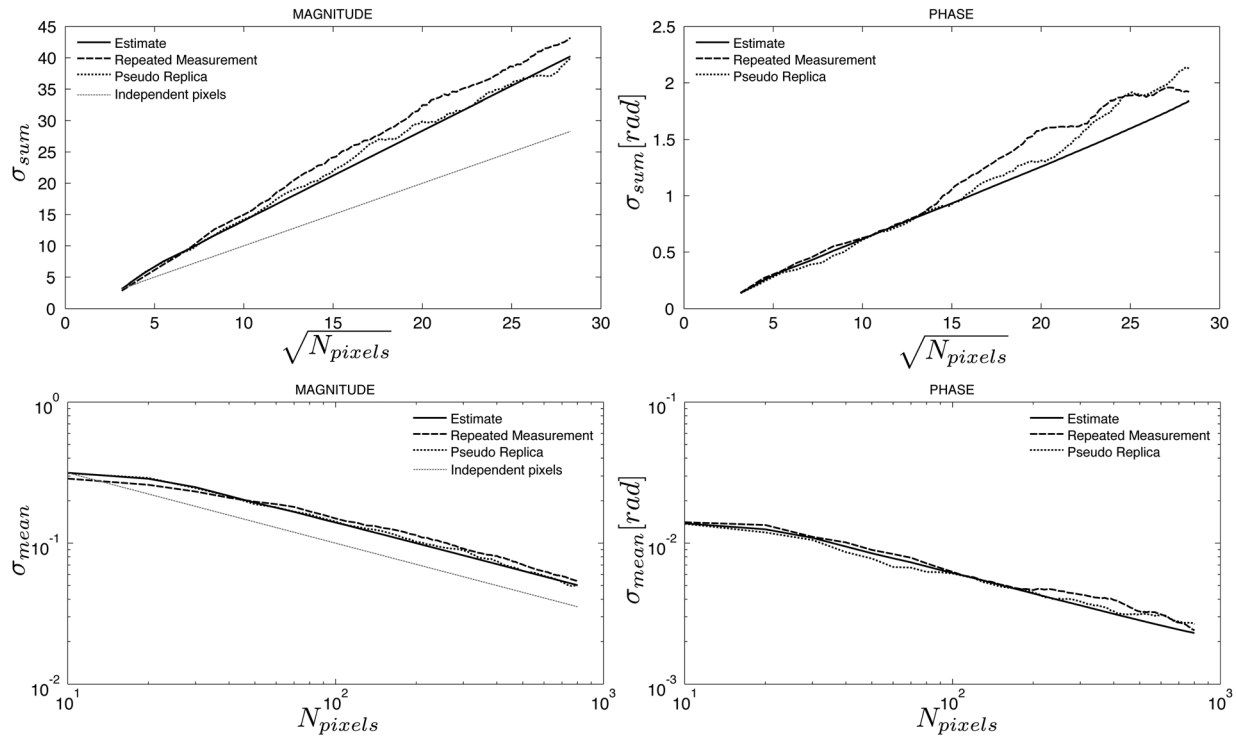

FIG. 5. Measured and predicted standard deviations (SD) of the sum (top row) and mean (bottom row) of a region of interest (ROI) as a function of the number of pixels in the ROI as it grows along the *phase-encoding* direction in an image with reduced effective resolution in the phase-encoding direction. The solid line is the predicted SD from the proposed method. The dashed line is the calculated SD from 100 repeated experiments. The dotted line is the calculated SD from 100 pseudo replica reconstructions. The gray dotted line on the magnitude plots indicated the predicted SD when assuming that all pixels are independent. Compared to Figure 4, the actual SDs and the gray line are in agreement for an ROI with length 1, but deviate as the ROI increases in length.

The results of the in vivo perfusion example are shown in Figure 8. The top row shows example frames from the series of real-time images acquired during infusion of a bolus of Gd contrast agent. A clear perfusion defect is present in the septal wall. The plot shows the individual time intensity curves of the hypoperfused and the healthy myocardium. The gray shaded areas indicate the 95% confidence interval ($\pm 1.96 * \sigma$) predicted by the proposed method, and the actual error bars represent the 95% limits of agreement calculated from 100 pseudo replica experiments. There is no practical way of measuring the 95% confidence interval from repeated measurements in the in vivo case, but the limits predicted by the proposed method and the ones obtained from the pseudo replica reconstructions are in good agreement. Fluctuations in the time intensity curves due to uncorrected respiratory motion are apparent; they are not caused by thermal noise.

DISCUSSION

Region of interest analysis is an important part of many MRI exams. Signal intensities of healthy and diseased tissues often are compared. In such analysis, it is advantageous to have an estimate of the SD of the sum or the mean of a given ROI caused by thermal noise propagation. In cases in which the pixels in the reconstructed image are independent, it is trivial to obtain such an estimate. Even in cases in which there is some easily predicted correlation between the pixels, it is fairly straightforward to predict the actual SD of ROI measurements—as illustrated in the experiment with reduced phase-encoding direction resolution (Figs. 4 and 5). However, some care still must be taken because the orientation of the ROI can affect the correlation between the pixels. In other cases, such as the parallel imaging example presented here (Figs. 6 and 7), the noise behavior is less intuitive and is influenced by things like the parallel imaging undersampling pattern, the actual phase of the signal in the images, and orientation of the ROI. This is especially true if the ROI covers a region of the FOV, which is larger than the FOV divided by the acceleration factor. Although it may be unusual to have ROIs that are large enough individually for these effects to become visible, it could have an effect on an ROI measurement for which two more distant regions of the image are compared.

The method described here provides a general way of calculating the SD of any linear combination of the pixels in an image. The method uses information about the reconstruction process to predict what the noise correlation of a linear transform of the k-space samples (where the noise is uncorrelated) would be. The method is intuitive in the sense that Eqs. [3], [9], and [10] can be thought of as assuming that the pixels are uncorrelated in the image and convolving them with the point spread

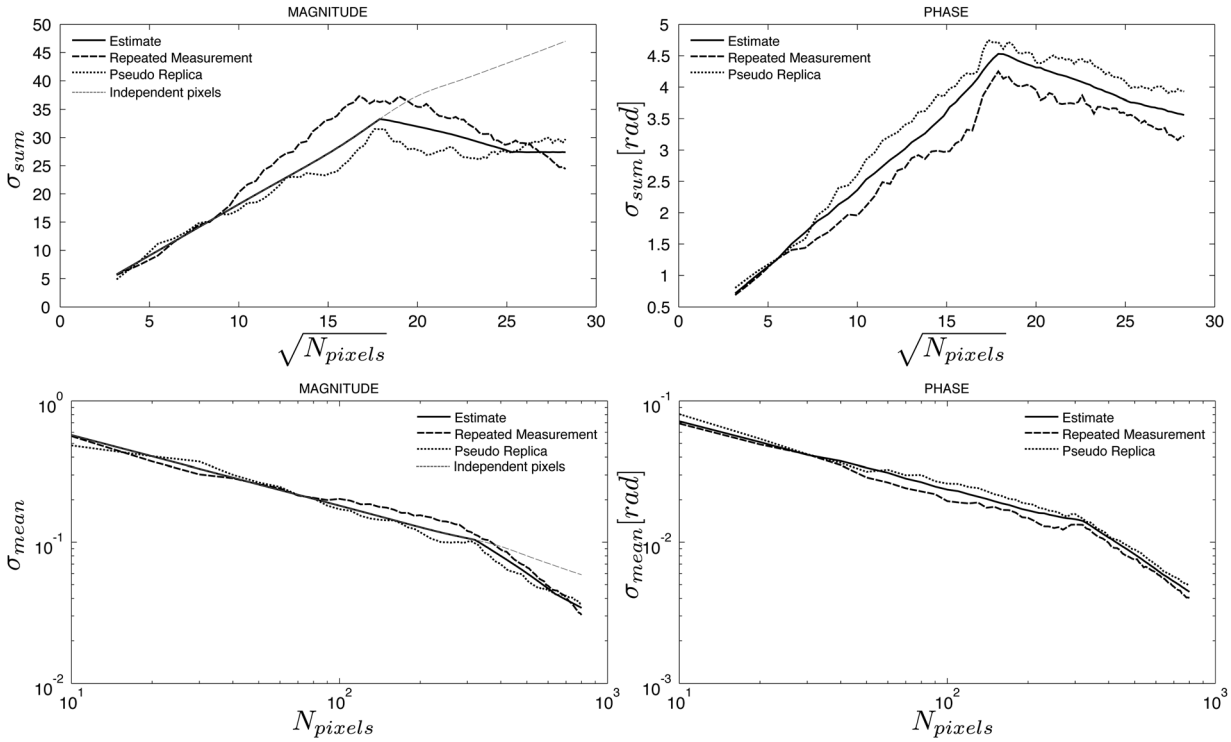

FIG. 6. Comparison of predicted and measured standard deviations (SD) of the sum (top row) and mean (bottom row) of a region of interest as it grows along the phase-encoding direction in an image with parallel imaging factor 4. The sampling pattern used here sampled lines 1, 5, 9, . . ., etc. The solid line is the predicted SD from the proposed method. The dashed line is the calculated SD from 100 repeated experiments. The dotted line is the calculated SD from 100 pseudo replica reconstructions. The gray dotted line on the magnitude plots indicated the predicted SD when assuming that all pixels are independent; that is, the SD is calculated based on the g-factor, taking parallel imaging-associated noise enhancement into consideration.

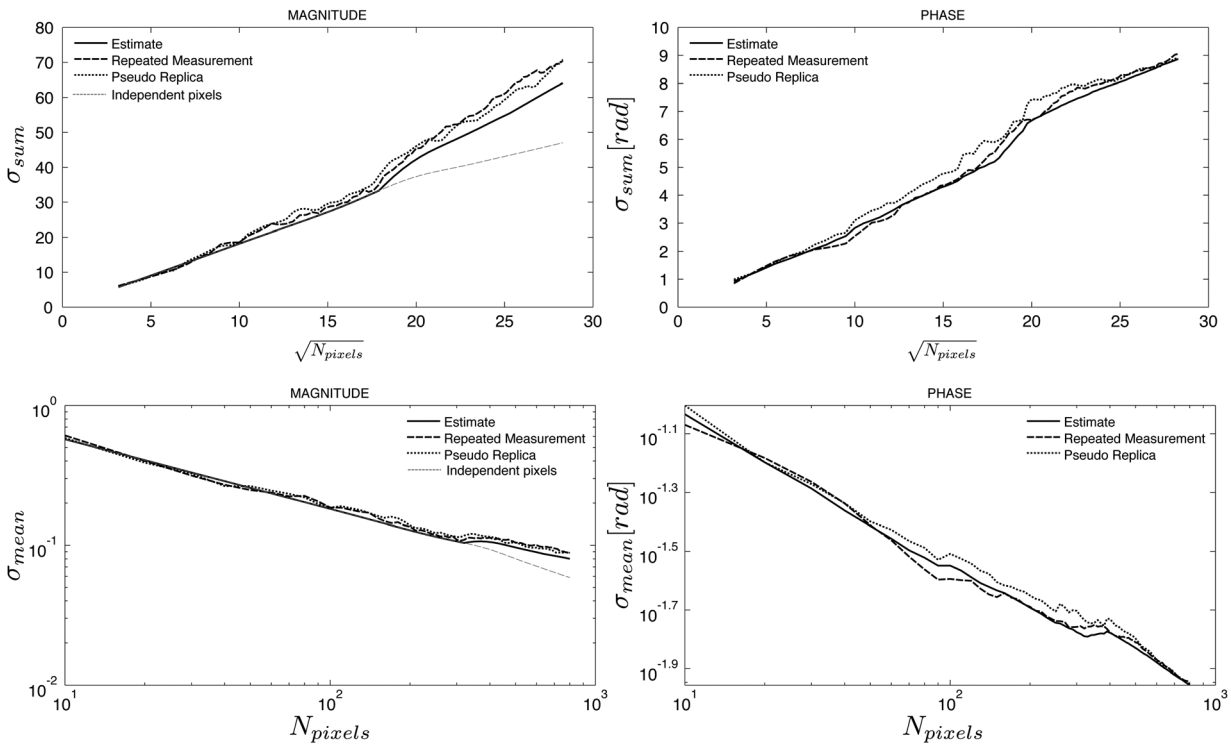

FIG. 7. Comparison of predicted and measured standard deviations (SD) of the sum (top row) and mean (bottom row) of a region of interest as it grows along the phase-encoding direction in an image with parallel imaging factor 4. Plot is similar to Figure 6, but the sampling pattern used here sampled lines 3, 7, 11, . . .; that is, the sampling pattern was still undersampled by a factor of 4, but the sampled lines were shifted by 2 lines in k-space.

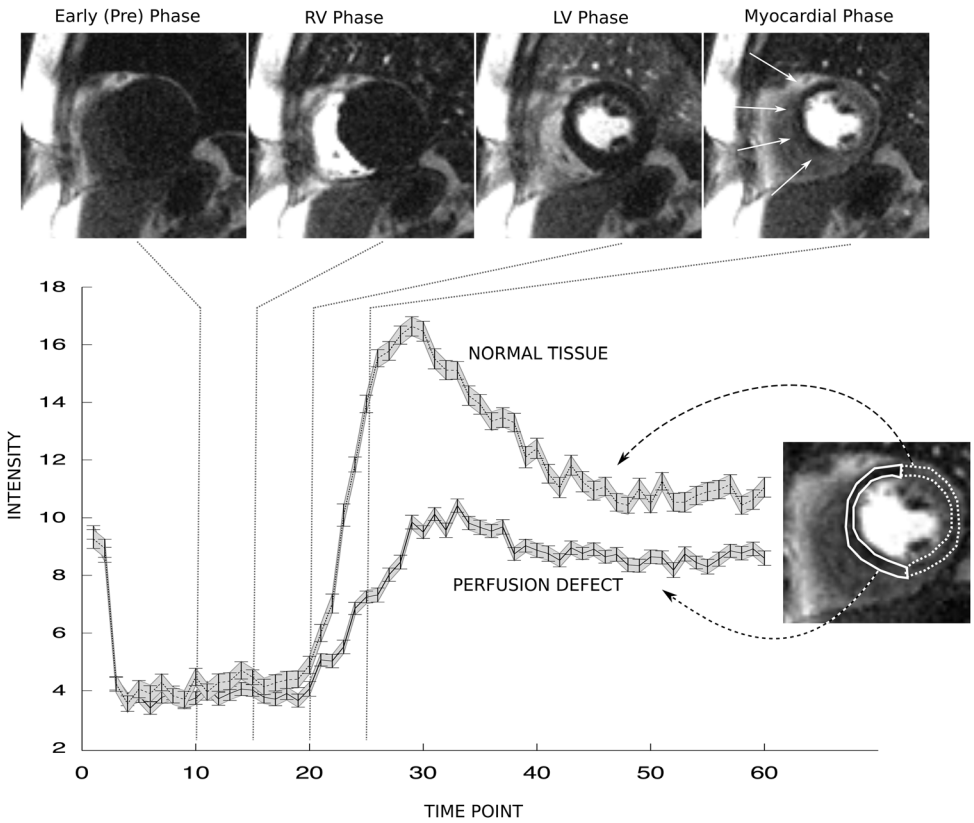

FIG. 8. Example of SD analysis on a stress perfusion MRI examination. The top row shows example real-time frames acquired during injection of a bolus of Gd contrast agent. The last frame shows a hypointense region in the septal wall marked by arrow. The plot on the bottom row shows time-intensity curves of the average signal in the region of interests (ROIs) drawn on the frame to the right of the curves. The solid line ROI contained the tissue with the perfusion defect, and the dotted line ROI contained the healthy tissue. The 95% confidence intervals ($\pm 1.96 * \sigma$) predicted by the proposed method are shown as the shaded gray area around the curve, and the 95% confidence intervals measured from 100 pseudo replicas are shown as the error bars on the curves.

function caused by the sampling and reconstruction. We have demonstrated that the method can be used to predict the SD in ROI measurements for both magnitude and phase measurements, even in the fairly complicated case of noise correlation caused by parallel imaging. A number of experimental and reconstruction parameters such as sampling pattern, calibration scheme, and GRAPPA kernel configuration (size) have an effect on the ROI noise propagation. The proposed method can be used to investigate the optimal settings of such parameters, although that was not explored here. The method is also able to predict SD in ROI measurements of real and imaginary parts of the signal (using Eq. [3]), but the plots were left out here due to their repetitive nature. The method uses some approximations for the nonlinear steps of extracting the magnitude and the phase during image reconstruction. These approximations rely on estimates of the image signal and phase, which may not be reliable in the case of low SNR. In the phantom experiments conducted here, the base SNR was on the order of 15 for the fully sampled case and considerably lower in the parallel imaging case, and the method was still able to predict the ROI noise behavior. In the case of lower SNR, it may be necessary to replace the approximation used for the estimation of phase SD ($\sigma_{phase} \sim \frac{1}{SNR}$) with a lookup table that takes the nonlinear increase in σ_{phase} at low SNR into account. In the studies conducted here, it was not found to be necessary, but the ultimate SNR limits of the proposed method were not explored in detail.

The method was compared here to both pseudo replica experiments, and actual repeated measurements in the case of the phantom study. The repeated measurements are rarely practical to perform (even in the case of phantom experiments), but the pseudo replica method is often an available option. Compared to the pseudo replica method, the proposed method is orders of magnitude faster and has a much smaller memory footprint, but it is only really practical for Cartesian measurements. Furthermore, the method requires detailed knowledge of the reconstruction process, which is not needed by the pseudo replica method in which the reconstruction can be treated as a black box. For non-Cartesian methods and when the reconstruction details are unknown, the pseudo replica method may be the only available option. In principle, the formulas in Eqs. [3], [9], and [10] are valid for non-Cartesian methods, but because pixel-wise unmixing coefficients are not generally obtained with non-Cartesian parallel-imaging reconstructions, they would be so computationally inefficient that the pseudo

replica method would the method of choice. The alternative to the pseudo replica method proposed by Wiens et al. (4) offers computational efficiency and is related to the method proposed in this article in that a region of the image is used to obtain a SD estimate. That method could be modified to obtain an ROI SD estimate if the image region used for smoothing was adapted to fit the ROI of interest, but the precision of the ROI SD estimate would suffer because only two (or a few) pseudo replicas would form the basis of the estimate.

In practice, ROI measurements are often done using an image analysis workstation operating on reconstructed images (in digital imaging and communications in medicine [DICOM] format). The proposed method and the pseudo replica method require access to the acquisition raw data and the reconstruction process. Consequently, there are some hurdles to the integration of such an analyses in a clinical workflow. However, the proposed method can potentially be integrated into an image analysis workstation if the infrastructure is available to store the image formation matrix (**F** in the equations above), the sampling pattern, and the complex images. The image formation matrix need not be stored in matrix form; it can be stored as a compiled function or script. If that information is available, the technique is fast enough that it can be applied on the fly during image analysis, and it does not require storage of multiple pseudo replica images.

CONCLUSION

This article proposes a method for the calculation of the SD of any linear combination the image pixels of a Cartesian MRI acquisition. The method accurately predicts SDs of region-of-interest measurements of complex, magnitude, and phase images.

ACKNOWLEDGMENTS

This research was supported by the Intramural Research Program of the National Institutes of Health; the National Heart, Lung, and Blood Institute; and the National Institute of Mental Health.

REFERENCES

1. Kellman P, McVeigh ER. Image reconstruction in SNR units: a general method for SNR measurement. Magn Reson Med 2005;54:1439–1447.
2. Kellman P, McVeigh ER. Erratum: Image reconstruction in SNR units: a general method for SNR measurement. Magn Reson Med 2007;58:211–212.
3. Robson PM, Grant AK, Madhuranthakam AJ, Lattanzi R, Sodickson DK, McKenzie CA. Comprehensive quantification of signal-to-noise ratio and g-factor for image-based and k-space-based parallel imaging reconstructions. Magn Reson Med 2008;60:895–907.
4. Wiens CN, Kisch SJ, Willig-Onwuachi JD, McKenzie CA. Computationally rapid method of estimating signal-to-noise ratio for phased array image reconstructions. Magn Reson Med 2011;66:1192–1197.
5. Sodickson DK, Manning WJ. Simultaneous acquisition of spatial harmonics (SMASH): fast imaging with radiofrequency coil arrays. Magn Reson Med 1997;38:591–603.
6. Pruessmann KP, Weiger M, Scheidegger MB, Boesiger P. SENSE: sensitivity encoding for fast MRI. Magn Reson Med 1999;42:952–962.
7. Griswold MA, Jakob PM, Heidemann RM, et al. Generalized autocalibrating partially parallel acquisitions (GRAPPA). Magn Reson Med 2002;47:1202–1210.
8. Pruessmann KP, Weiger M, Börnert P, Boesiger P. Advances in sensitivity encoding with arbitrary k-space trajectories. Magn Reson Med 2001;46:638–651.
9. Williams DF, Lewandowski A, Clement TS, et al. Covariance-based uncertainty analysis of the NIST electrooptic sampling system. IEEE Trans Microw Theory Tech 2006;54:481–491.
10. Lequin RM. Guide to the expression of uncertainty of measurement: point/counterpoint. Clin Chem 2004;50:977–978.
11. Williams DF, Wang CM, Arz U. In-Phase/Quadrature covariance-matrix representation of the uncertainty of vectors and complex numbers. Presented at: 68th ARFTG Microwave Measuring Conference: measuring for emerging technologies, Broomfield, Colorado, USA, 2006.
12. Breuer FA, Kellman P, Griswold MA, Jakob PM. Dynamic autocalibrated parallel imaging using temporal GRAPPA (TGRAPPA). Magn Reson Med 2005;53:981–985.
13. Walsh DO, Gmitro AF, Marcellin MW. Adaptive reconstruction of phased array MR imagery. Magn Reson Med 2000;43:682–90.
14. Kellman P, Epstein FH, McVeigh ER. Adaptive sensitivity encoding incorporating temporal filtering (TSENSE). Magn Reson Med 2001;45:846–52.